CARBON letters

Original Articles
Carbon Letters Vol. 25, 68-77 (2018)

Carbon molecular sieves from soybean straw-based activated carbon for CO_2/CH_4 separation

Yuxian Xu[1,2,*], Xiaochuan Chen[1,2], Dan Wu[1,2], Yongjin Luo[1,2], Xinping Liu[1,2], Qingrong Qian[1,2,♠], Liren Xiao[2,3] and Qinghua Chen[1,2,4,♠]

[1]College of Environmental Science and Engineering, Fujian Normal University, Fuzhou 350007, China
[2]Fujian Key Laboratory of Pollution Control & Resource Reuse, Fuzhou 350007, China
[3]College of Materials Science and Engineering, Fujian Normal University, Fuzhou 350007, China
[4]Fuqing Branch of Fujian Normal University, Fuqing, Fujian 350300, China

Article Info
Received 2 June 2017
Accepted 25 August 2017

♠Corresponding Author
E-mail: qrqian@fjnu.edu.cn
E-mail: cqhuar@fjnu.edu.cn
Tel: +86-591-8346-5158
*The authors have contributed equally in discussions of the work, performing the experiments, and writing the paper.

DOI: http://dx.doi.org/10.5714/CL.2018.25.068

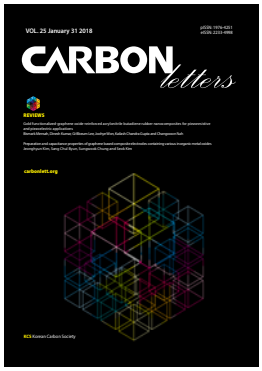

http://carbonlett.org

pISSN: 1976-4251
eISSN: 2233-4998

Abstract

Soybean straw (SS)-based activated carbon was employed as a precursor to prepare carbon molecular sieves (CMSs) via chemical vapor deposition (CVD) technique using methane as carbon source. Prior to the CVD process, SS was activated by 0.5 wt% $ZnCl_2$, followed by a carbonization at 500°C for 1 h in N_2 atmosphere. N_2 (77 K) adsorption-desorption and CO_2 (273 K) adsorption tests were carried out to analyze the pore structure of the prepared CMSs. The results show that increasing the deposition temperature, time or methane flow rate leads the decrease in N_2 adsorption capacity, micropore volume and average pore diameter of CMSs. The adsorption selectivity coefficient of CO_2/CH_4 achieves as high as 20.8 over CMSs obtained under the methane flow rate of 30 mL min^{-1} at 800°C for 70 min. The study demonstrates the prepared CMSs are a candidate adsorbent for CO_2/CH_4 separation.

Key words: activated carbon, adsorption properties, chemical vapor deposition, microporosity

1. Introduction

Biogas is considered to be a promising renewable and low-carbon energy source, which can be substituted for fossil fuels in power and heat production, and also can be used as gaseous vehicle fuel. Moreover, methane-rich biogas can replace natural gas as a feedstock for producing chemicals and materials [1,2]. However, biogas contains unacceptable levels of contaminants, which consists of approximately 40% CO_2. Removing CO_2 from biogas will enhance energy content and prevent corrosion of pipelines, which is critical for the gas transportation system [3,4]. Thus, the separation of CO_2 from methane is essential for upgrading of biogas and reduction of pipeline corrosion caused by acid CO_2 gas [5,6]. Various technologies such as chemical separation, membrane separation, cryogenic separation and adsorption are employed to separate CO_2 from biogas [7]. Pressure swing adsorption (PSA) is known as an energy efficient gas separation technology for biogas purification and separation [8]. Carbon molecular sieves (CMSs) that have highly developed porous structure and special surface features can separate one kind of chemical from the mixed gas, making it become the first-choice material for the PSA technology [9]. For these applications, CMSs must possess a narrow pore size distribution centered in a molecular size and a relatively high micropore volume, which confer them selectivity and capacity, respectively [10]. Besides, CMSs should give high adsorption and desorption rates, as the performance for PSA cycles designed for kinetic separation is usually optimal for cycles with short time duration [11].

Our previous experiment has proved that activated carbon (AC) derived from soybean straw (SS) that activated by $ZnCl_2$ possesses high specific surface area [12]. It is a suitable

precursor for CMS. During the CVD approach, carbons can deposit at the micropore mouths of AC and reduce the pore size, thus yielding CMS. The carbonaceous substances usually including those of benzene [13,14], acetylene [15], furfuryl alcohol [16], and methane [17,18]. Ahmad [14] reported that CMS prepared from palm shell through carbonization, steam activation and CVD treatment with benzene has an uptake ratio of 16.0 for CO_2/CH_4. Due to the high toxicity of benzene and the complexity of operation, methane is gradually used to displace benzene.

Hence, this study employed SS as a precursor to prepare CMSs by using $ZnCl_2$ as an activating agent in the activation process and methane as a carbon source in the CVD process. The influence of ZnCl impregnation ratio, deposition temperature, time and methane flow rate on the pore structure and the adsorption behavior of the prepared CMSs were discussed, and the adsorption selectivity coefficient of CO_2/CH_4 over CMSs at 273 K was also investigated.

2. Experimental

2.1. Preparation

2.1.1. Preparation of soybean straw-based activated carbon

The preparation of SS-based AC was according to our previous report [12]. $ZnCl_2$ was dissolved in distilled water to prepare a $ZnCl_2$ solution. Then the approximate amount of SS particles was mixed with $ZnCl_2$ solution and stirred for 12 h. The homogeneous mixture was dried in an oven at 105°C prior to carbonization. The carbonization was carried out at 500°C for 1 h under the N_2 flow rate of 300 mL min^{-1}. The resultant AC was washed with 3 mol L^{-1} HCl solution by heating at around 70°C for 30 min, filtered and rinsed by warm distilled water until the washed solution was free of zinc ions, subsequently dried at 105°C for 12 h and sieved out in the range of 20–300 mesh. ZnCl activated ACs with $ZnCl_2$/SS mass ratios (impregnation ratios) of 0, 0.5, 1.0 and 2.0 were denoted as ZnS0.0, ZnS0.5, ZnS1.0 and ZnS2.0, respectively.

2.1.2. Preparation of CMSs

About 0.5 g AC was put into the quartz boat and loaded into the horizontal tubular furnace, first purged with N_2 gas at a flow rate of 200 mL min^{-1} for 30 min, then followed by heating up to the deposition temperature with a heating rate of 10°C min^{-1}. Then the N_2 flow rate was adjusted from 200 to 100 mL min^{-1} and methane gas was introduced with the flow rates ranging from 0 to 30 mL min^{-1}. The CVD experiments were performed under the mixed gas flow at various temperatures for various times. The obtained samples were referred to as CMSs followed by the deposition temperature, holding time and the methane flow rate. For instance, CMS80060-20 represents that carbon deposits on AC at 800°C for 60 min with a methane flow rate of 20 mL min^{-1}.

2.2. Characterization

The specific surface area and the pore characteristic of the samples were measured on a BELSORP-mini surface area analyzer (BELSORP Co., Japan) using N_2 adsorption-desorption at 77 K. The samples were degassed at 527 K for 180 min prior to the experiment. The surface area was estimated by Brunauer-Emmett-Teller (BET) method. The total volume (V_{total}) was obtained by the gas volume adsorbed at a relative pressure of 0.99, and the pore size distribution was investigated based on the non-local density functional theory (NLDFT) model [19]. In addition, the Dubinin-Radushkevich (DR) equation was applied to calculate the micropore volume according to N_2 and CO_2 adsorption isotherms [20]. The adsorption isotherms of CH_4 and CO_2 at 273 K were obtained on the BELSORP-mini apparatus to analyze the separation property of CMSs, and the adsorption selectivity coefficient of CO_2/CH_4 was calculated.

The phases of samples were determined on an X-ray diffraction analyzer (XRD, D8 Advance, Bruker, USA) using graphite monochromatized Cu Kα radiation, the accelerating voltage and the applied current were 40 kV and 40 mA. The morphology and microstructure of the samples were analyzed on a field emission scanning electron microscope (FESEM; Hitachi SU8010, Japan) and a transmission electron microscope (TEM; Tecnai G2, FEI), respectively. The thermogravimetric analysis was performed using a Derivatograph TGA Q50 (TA instruments, USA) with simultaneous recording of thermogravimetry (TG) curves in relation to temperature and time (N_2 atmosphere: heating rate, 10°C/min; temperature range, 25–800°C).

2.3. Gas adsorption-desorption measurements

The CH_4 and CO_2 adsorption-desorption rates measurements were performed on a TCD gas chromatograph. 0.2 g sample was heat-treated under an inert gas at 300°C for 0.5 h prior to the adsorption-desorption experiment. The CH_4 and CO_2 adsorption-desorption was performed at 273 K. In adsorption rates measurement, the feed gas (CH_4 or CO_2) flow rate was 4 mL min^{-1}. While adsorption saturation was reached, the feed gas was switched to inert gas (6 mL min^{-1}) to measure desorption rates. The adsorption/desorption rate was reported as C/C_0, where C and C_0 were the outlet CO_2 or CH_4 concentration at a given time and the beginning, respectively.

2.4. Virial graph analyses [21]

The virial equation can be employed to analyze the isotherm data

$$\ln (n/p) = A_0+A_1n+A_2n^2 +\ldots \quad (1)$$

At the low surface coverage, the equation can be written:

$$\ln (n/p) = A_0+A_1n \quad (2)$$

where n is the adsorbed amount, p is pressure, A_0 describes adsorbate−adsorbent interactions, and A_1 is related to adsorbate−adsorbate interactions. The Henry's law constant (K_H) is equal to exp (A_0).

Table 1. The properties of ACs with different impregnation ratio

ACs	S_{BET} ($m^2\ g^{-1}$)	V_{total} ($cm^3\ g^{-1}$)	V_{mi} ($cm^3\ g^{-1}$)	Microporosity
ZnS0.0	406	0.1574	0.1272	81%
ZnS0.5	1615	0.5737	0.5214	91%
ZnS1.0	2735	0.9426	0.7050	75%
ZnS2.0	1767	1.5497	0.6586	42%

Zn, represents $ZnCl_2$; S, represents soybean straws, and numeric represents impregnation ratios.

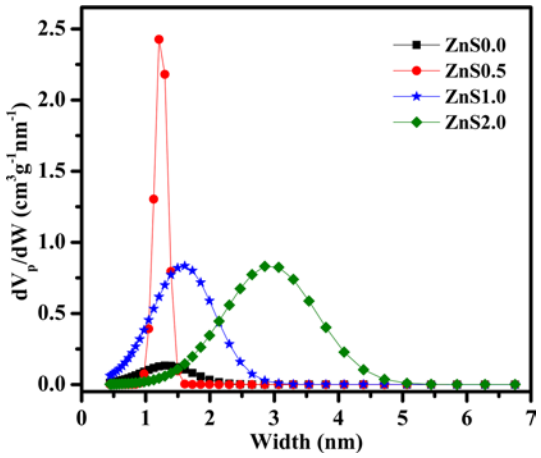

Fig. 1. NLDFT pore size distribution curves for various ACs obtained at various $ZnCl_2$ impregnation ratios.

3. Results and Discussion

3.1. Effect of different parameters for CMSs

3.1.1. $ZnCl_2$ impregnation ratio

A reasonably high porosity of AC is essential for preparing CMSs. In our experiments, $ZnCl_2$ is used as an activation agent because it can produce carbon materials with large micropore volume [22]. Table 1 lists the properties of ACs with different ZnCl impregnation ratios. The presence of $ZnCl_2$ can significantly improve the specific surface area (S_{BET}) and the micropore volume (V_{mi}^{DR}) of carbon materials. This is due to the occurrence of $ZnCl_2$ reacting with AC atoms on the surface or at the edge of SS. Raising the $ZnCl_2$ impregnation ratio results in an increase in the total pore volume. When the $ZnCl_2$ impregnation ratio increases from 0.0 to 1.0, S_{BET} increases from 406 to 2735 $m^2\ g^{-1}$ and V_{mi}^{DR} enlarges from 0.1272 to 0.7050 $cm^3\ g^{-1}$. However, the S_{BET} and V_{mi}^{DR} decrease to 1767 $m^2\ g^{-1}$ and 0.6586 $cm^3\ g^{-1}$ at the impregnation ratio of 2.0, respectively. From NLDFT pore size distribution (Fig. 1), it can be found that the pore sizes of AC mainly focus on 1.0–1.5 nm at the $ZnCl_2$ impregnation ratio of 0.5. At the $ZnCl_2$ impregnation ratio of 1.0 and 2.0, the pore size distribution becomes wide; meanwhile, more mesopores (>2 nm) are present over ZnS2.0. Therefore, excess of $ZnCl_2$ will destroy the pores walls and transform parts of micropores into mesopores. For fabricating CMSs with super microporous structure, ZnS0.5 is chosen to further be modified by the heat and CVD process in the following experiments.

3.1.2. Heat treatment temperature

In order to obtain a themo-stable precursor, ZnS0.5 was

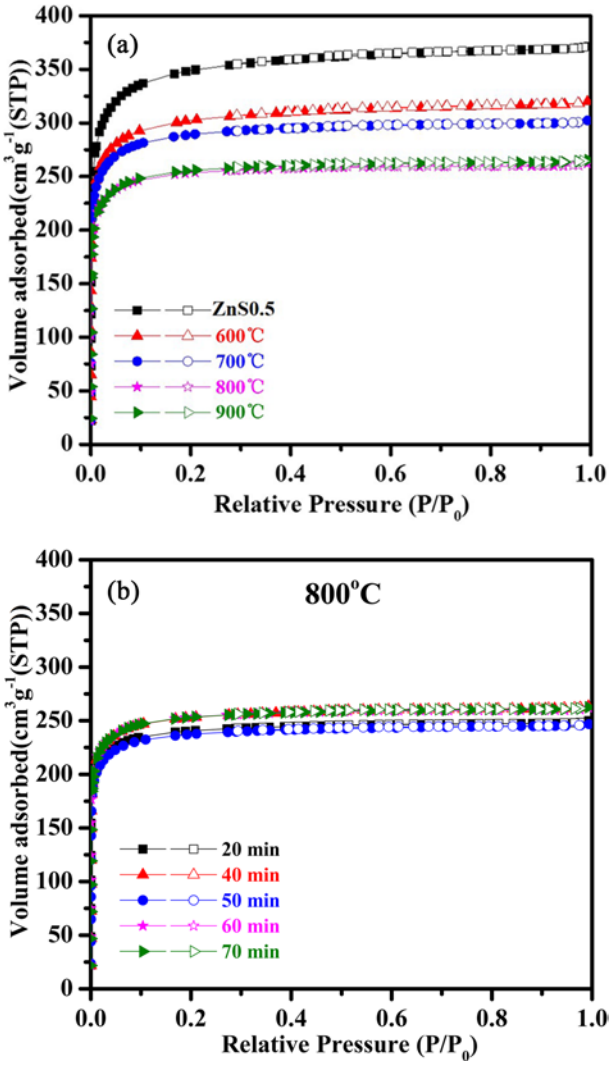

Fig. 2. The influence of different heat treatment conditions (a) and at 800°C for different times (b) on the pore structures of ACs. Open symbols, adsorption; closed symbols, desorption.

treated by heat prior to CVD. Fig. 2 illustrates the influence of different heat treatment conditions on ZnS0.5. In Fig. 2a, all N_2 adsorption-desorption curves exhibit a steep type I isotherm with a small hysteresis loop of type H_4, indicating the highly narrow pore size distribution microporous materials with slit-like or plate-like pores. It is worth pointing out that AC treated at 900°C for 60 min (Fig. 2a) gives almost the same isotherm profile as those treated at 800°C (Fig. 2b). On the other hand, heat treatment time affects little in their N_2 adsorption-desorption curves. It indicates that ACs treated at 800°C for 60 min can gain a thermostable pore structure, which is used as the CMS precursor and denoted as pretreated ACs.

3.1.3. Deposition temperature and time

The influence of various deposition temperatures on CMSs is shown Fig. 3. In Fig. 3a, all N_2 adsorption/desorption isotherms show a Type I curve, indicating the presence of micropores in CMSs. The N_2 adsorption/desorption isotherms have little difference among pretreated ACs, CMS60060-20 and CMS70060-20, suggesting that only a few carbons deposit on the surface of pretreated ACs. However, when the deposition temperature increases to 800°C, the N_2 adsorption/desorption isotherms decline obviously, indicating carbons have successfully deposited on CMSs.

In addition, CO_2 adsorption method was employed to investigate the super microporous structure of CMSs. The CO_2 adsorption isotherms of CMSs obtained at different deposition temperatures are given in Fig. 3b and the calculated values of the parameters are listed in Table 2. Pretreated ACs, CMS60060-20 and CMS70060-20 give an approximate CO_2 adsorption isotherm, revealing they have an approximate microporous structure. CMS80060-20 possesses a low CO_2 adsorption capacity due to the transformation of micropores

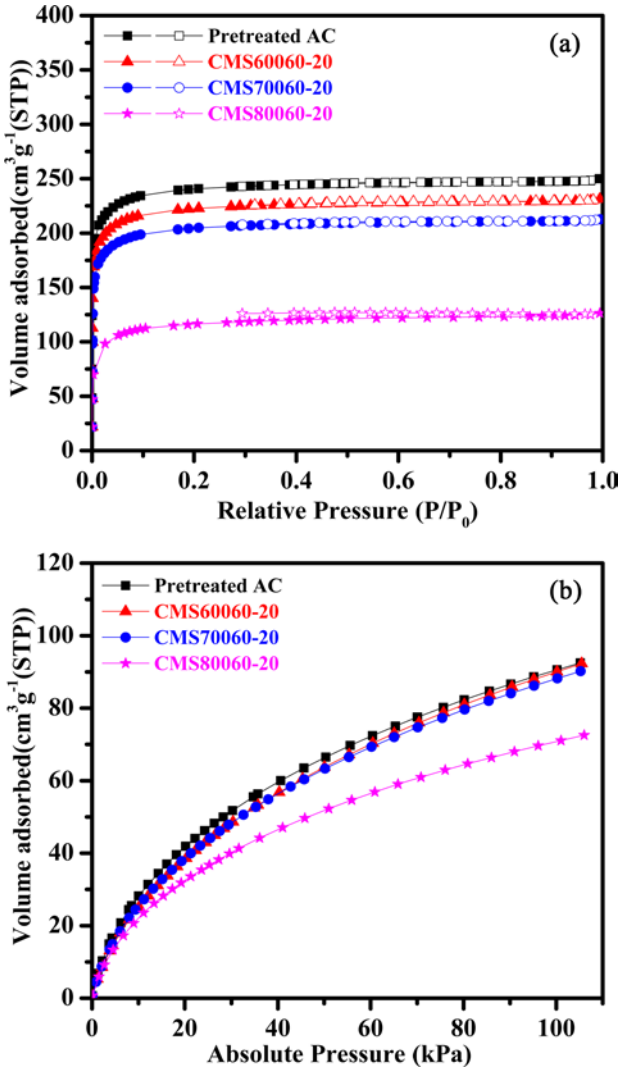

Fig. 3. The N_2 adsorption-desorption (a) and CO_2 adsorption isotherms (b) of CMSs derived from the AC by CVD at different deposition temperatures. Open symbols, adsorption; closed symbols, desorption.

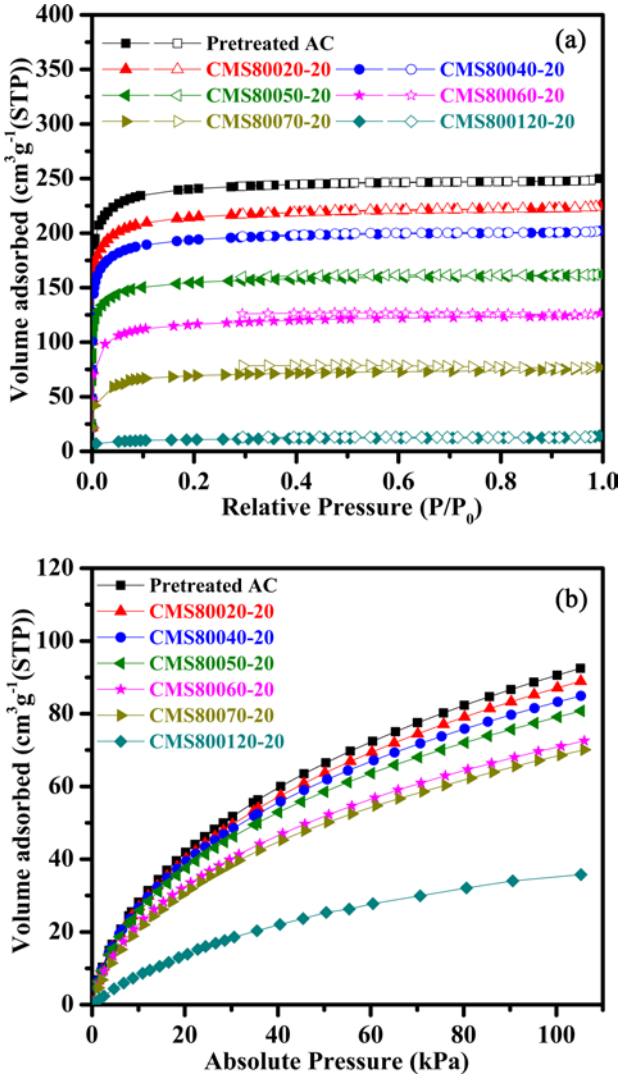

Fig. 4. The N_2 adsorption-desorption (a) and CO_2 adsorption isotherms (b) of CMSs derived from the AC by CVD at different deposition times. Open symbols, adsorption; closed symbols, desorption.

Table 2. The properties of CMS produced at different methane flow rates

Sample	N_2-adsorption			CO_2-adsorption
	S_{BET} (m^2 g^{-1})	V_{total} (cm^3 g^{-1})	V_{mi}^{DR} (cm^3 g^{-1})	V_{mi}^{DR} (cm^3 g^{-1})
Pretreated AC	1083.4	0.3862	0.3814	0.3359
CMS60060-20	1017.7	0.3624	0.3592	0.3260
CMS70060-20	922.5	0.3284	0.3251	0.3004
CMS80060-20	547.2	0.1950	0.1875	0.2429
CMS80020-20	973.1	0.3471	0.3411	0.3018
CMS80040-20	876.6	0.3122	0.3083	0.2799
CMS80050-20	704.0	0.2505	0.2464	0.2662
CMS80060-20	547.2	0.1950	0.1875	0.2429
CMS80070-20	325.3	0.1186	0.1128	0.2275
CMS800120-20	56.3	0.0215	0.0190	0.1374
CMS80070-10	786.5	0.2815	0.2768	0.2678
CMS80070-20	325.3	0.1186	0.1128	0.2246
CMS80070-30	20.4	0.008851	0.005319	0.2020
CMS80070-40	2.5	0.000427	0.000219	0.1262

into super micropores by the occurring of carbon deposition at 800°C.

Fig. 4 shows the N_2 adsorption/desorption isotherms and CO_2 adsorption isotherms of CMSs at 800°C for various deposition times. Clearly, the N_2 adsorption/desorption isotherms gradually decline with increasing the deposition time from 20 to 120 min (Fig. 4a), suggesting that long deposition time results in more carbon depositing on CMSs and reduction of pore size and pore volume. It is interesting that CMSs obtained at the deposition time of 60 and 70 min both give a misalignment of the adsorption isotherm and desorption isotherm branch, which is attributed to the formation of ink bottle-type pores in CMSs. The N_2 molecules adsorbed in this type of pores are not easily desorbed.

CO_2 adsorption isotherms of CMSs produced at various deposition times are illustrated in Fig. 4b. All CO_2 adsorption isotherms of CMSs decrease with increasing deposition time. However, the magnitude of decrement is lower than that of the N_2 adsorption/desorption isotherms. This phenomenon is evidenced by analyzing the properties of CMSs as given in Table 2. When the deposition time increases from 20 to 120 min, the adsorbed volumes of N_2 decrease from 0.3471 to 0.0215 cm^3 g^{-1}, whereas that of CO_2 from 0.3018 to 0.1374 cm^3 g^{-1}. It is because that methane adsorbed in pores of pretreated ACs is decomposed to carbons depositing on the interior wall, resulting in the decrement of pore size and pore volume at initial deposition time. When the deposition time prolongs to 120 min, carbon deposits at the edges of pore and forms the ink-bottle like pores, the pore size becomes too small to allow CO_2 molecules entering.

3.1.4. Methane flow rate

The methane flow rate also has an important effect on the pore size of CMSs. In Fig. 5a and Table 2, the N_2 adsorption capacity of CMSs declines with increase in methane flow rate. The CMSs obtained via CVD at the methane flow rate higher than 30 mL min^{-1} for 70 min show a low N_2 adsorption capacity, suggesting that the pores fit for N_2 adsorption in CMSs are constricted to form primary micropore or even blocked. However, the obtained CMSs with the methane flow rate higher than 30 mL min^{-1} still have a relatively high CO_2 adsorption capacity (Fig. 5b). So the pore size of CMSs can be effectively adjusted to separate gas by controlling the methane flow rate.

3.2. Structure and morphology characterization

Fig. 6 shows the TG curve of SS, SS/$ZnCl_2$ (0.5 wt%), ZnS0.5 and pretreated AC. The overall mass loss of SS during thermo-gravimetric analyses can be divided into steps related to the elimination of moisture, hemicellulose, cellulose and lignin. The initial weight loss occurs around 30–100°C, corresponding to the elimination of moisture retained in SS. The main decomposition step takes place between 210 and 360°C, which is caused by the pyrolysis of hemicellulose and cellulose. Finally, in the temperatures range of 30–100°C, the ~20% mass loss is associates with the decomposition of lignin [23].

In the case of SS/$ZnCl_2$, the decomposition takes place in four stages. The first stage also occurs at temperatures ranging from 30 to 100°C, involves the loss of residual water (8 wt%) presented in the sample. The decomposition of hemicellulose, cellulose and lignin occurs at lower temperature range of 100–

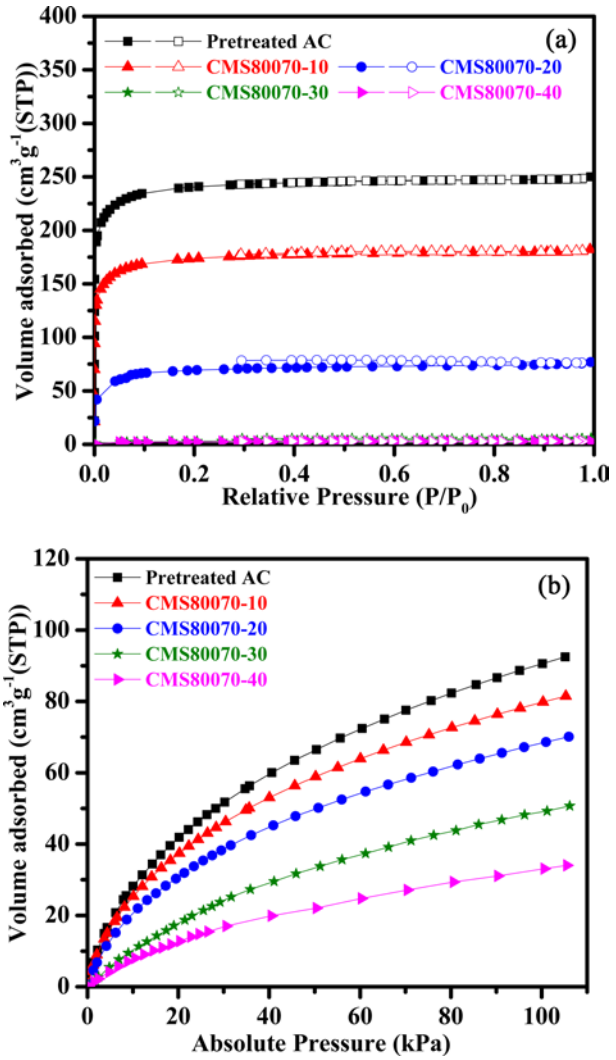

Fig. 5. The N_2 adsorption-desorption (a) and CO_2 adsorption isotherms (b) of CMSs derived from the AC by CVD at different methane flow rates. Open symbols, adsorption; closed symbols, desorption.

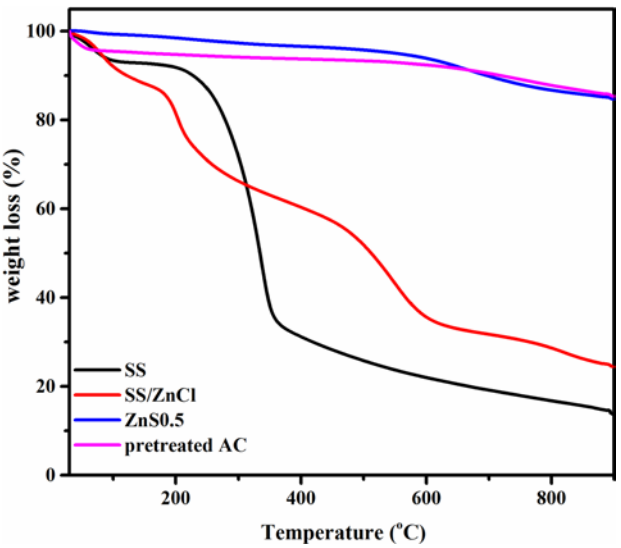

Fig. 6. TG curves of the samples.

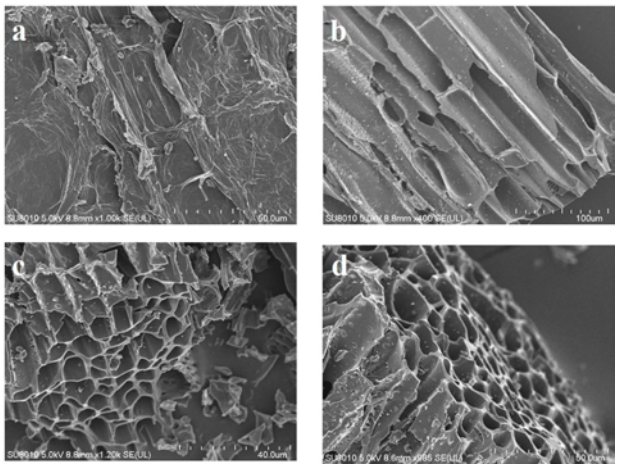

Fig. 7. SEM images of (a) SS, (b) ZnS0.5, (c) pretreated AC, and (d) CMS80070-30.

450°C. It is because the presence of $ZnCl_2$ had a significant effect on decomposition of SS by dehydration in low temperature and restricted the formation of tar at the same time, thus reducing the mass loss [24]. Further heated up to 600°C, 20% weight loss is ascribed to the release of $ZnCl_2$ and a few volatiles. In the range from 600 to 900ºC, the weight decreases slowly. Regarding ZnS0.5 and pretreated AC, they present residual masses of 84% and 85% at 900°C, respectively. The similar residual mass indicates that lignocellulosic materials can be degraded completely after procedures of activation by ZnCl solution and carbonization at 500ºC [25].

Scanning electron microscope is used to obtain information about the morphology of SS, ZnS0.5, pretreated AC and CMS80070-30. As can be seen in Fig. 7a, the SS surface appears rough. Because the complete degradation of lignocellulosic material occurs during activation procedures and carbonization, obvious hollow tunnels and porous structure are presented in ZnS0.5, which is beneficial to gas transmission and contributes to large surface areas. The porous structure stems from the evaporation of $ZnCl_2$ after the acid washing, leaving the void space previously occupied by $ZnCl_2$ [12]. Pretreated AC and CMS80070-30 present similar morphologies as ZnS0.5, indicating heat and CVD treatment have no visual effect on the surface morphology. It also suggests that ZnS0.5 exhibits high stability. The high resolution of TEM images show ZnS0.5, pretreated AC and CMS80070-30 exhibit worm-like micropores, and the pore sizes of most micropores are less than 1 nm (Fig. 8) [26].

The XRD patterns of ACs and CMSs are displayed in Fig. 9. It is observed that ZnS0.0 exhibits two broad peaks appeared at approximately 2θ=23.5° and 43.5°, which are attributed to the presence of amorphous (002) and graphitic (100) carbons, respectively [27]. The XRD patterns change little for ACs (Fig. 9a). It indicates that activation parameters have little effect on the structure of formed AC. However, as seen in Fig. 9b, the

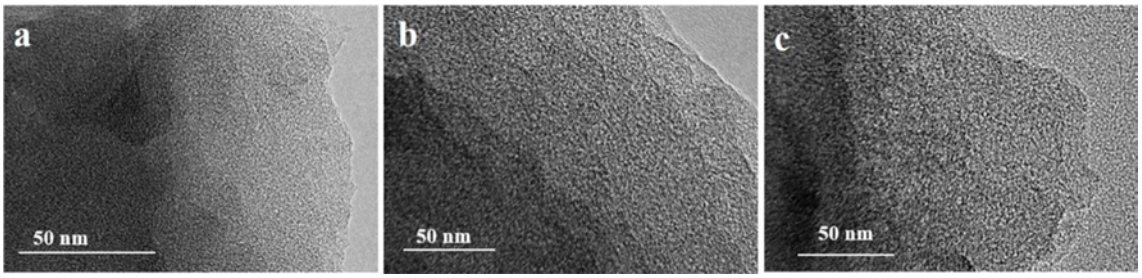

Fig. 8. TEM images of (a) ZnS0.5, (b) pretreated AC, and (c) CMS80070-30.

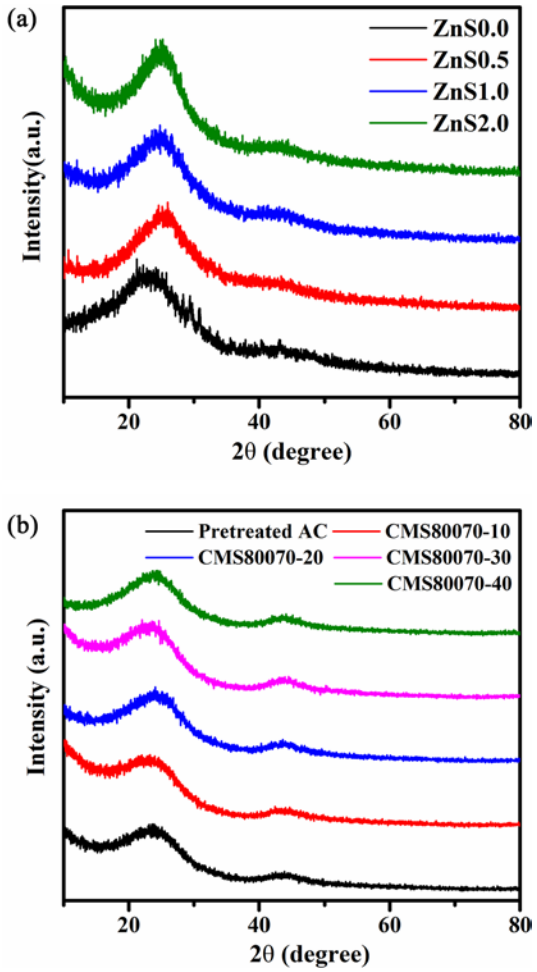

Fig. 9. XRD patterns of (a) ACs, and (b) pretreated AC and CMSs.

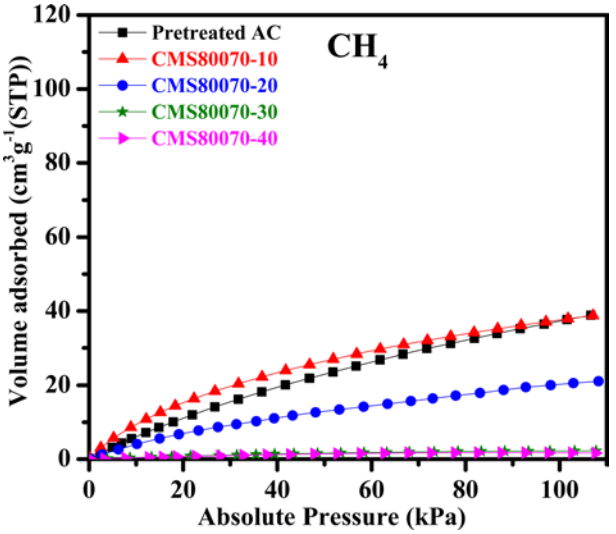

Fig. 10. The adsorption isotherms of CH_4 on different CMSs at 273 K.

peak intensity of graphitic (100) carbons phase is increased after heat and CVD treatment. It indicates pretreated AC and CMSs are more stable than ZnS0.5.

3.3. CO_2/CH_4 separation property

In order to investigate the adsorption selectivity of CO_2/CH_4 for prepared CMSs, the CH_4 adsorption experiments were also performed, and the results are given in Fig. 10. As shown in Fig. 5b and Fig. 10, the adsorption capacity of CO_2 and CH_4 decrease with an increase in the methane flow rate in the CVD process, revealing that the carbon deposition on CMSs can reduce both pore diameter and pore volume.

The adsorption selectivity coefficients (α) of CO_2 and CH_4 can be obtained from the Henry's law constants (K_H), using the following equation:

$$\alpha = K_{H(CO2)} / K_{H(CH4)} \quad (3)$$

The adsorption selectivity coefficients of CO_2/CH_4 on different CMSs are listed in Table 3. The adsorption selectivity coefficient for CO_2/CH_4 on pretreated AC is 3.0, which slightly decreases to 2.9 for CMS80070-10. However, it significantly increases to 7.0, 20.8 and 17.2 under the methane flow rates of 20, 30 and 40 mL min^{-1}, respectively. It is suggested that increasing methane flow rate results in the increment of carbon deposition and the transformation of micropore to supermicropore, resulting in the decrease in both of the adsorption capacity for CO_2 and CH_4. To be mentioned, the decrement of CH_4 adsorption is higher than that of CO_2 adsorption due to the larger molecular size of CH_4. Both the adsorption capacity for CO_2 and CH_4 are found to be low on CMS80070-40 due to the blocked supermicropore by carbon. There are few pores allowing CH_4 or CO_2 molecule to enter.

It is generally believed that two gases can be separated

Table 3. Analysis of CH_4 and CO_2 adsorption isotherms at 273 K

Adsorbate	Sample	A_0/ln(mmol g^{-1} Pa^{-1})	K_H/mmol g^{-1} Pa^{-1}	α
CO_2	Pretreated AC	–2.723	0.066	
	CMS80070-10	–2.829	0.059	
	CMS80070-20	–3.800	0.022	
	CMS80070-30	–5.905	0.003	
	CMS80070-40	–6.257	0.002	
CH_4	Pretreated AC	–1.639	0.194	3.0
	CMS80070-10	–1.748	0.174	2.9
	CMS80070-20	–1.847	0.158	7.0
	CMS80070-30	–2.870	0.057	20.8
	CMS80070-40	–3.410	0.033	17.2

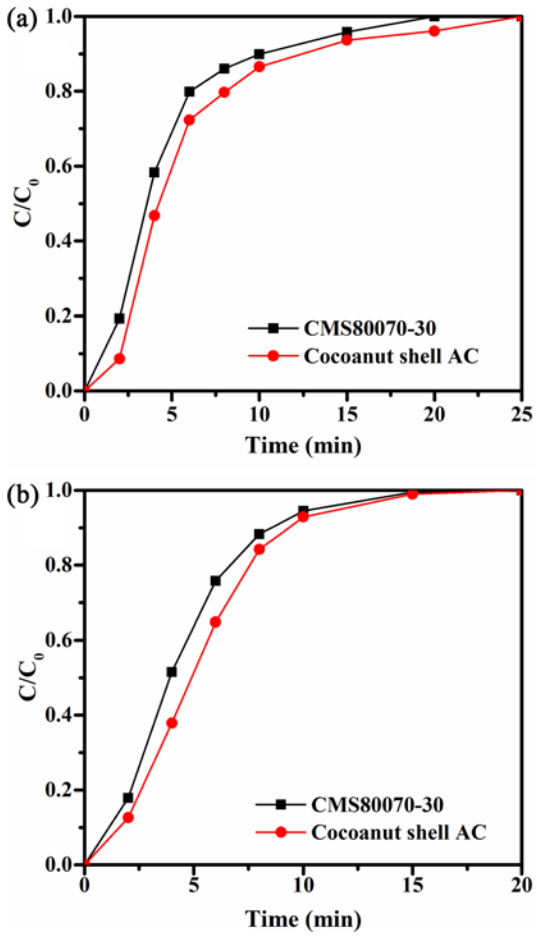

Fig. 11. Gas adsorption rates of CMS80070-30 and cocoanut shell AC. (a) CH_4 and (b) CO_2.

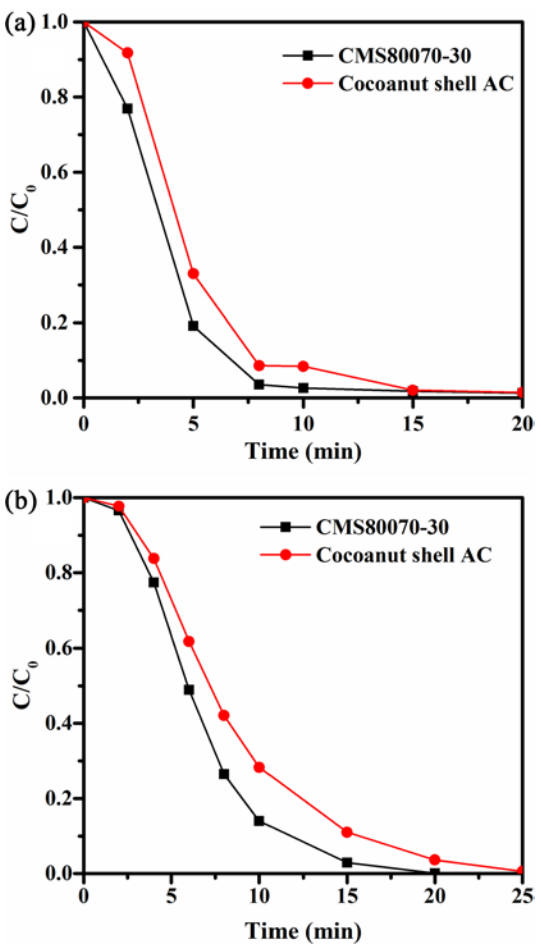

Fig. 12. Gas desorption rates of CMS80070-30 and cocoanut shell AC. (a) CH_4 and (b) CO_2.

with an adsorbent by means of PSA in industrial scale if they have an adsorption selectivity coefficient above 3.0 [4]. Accordingly, CMSs obtained from SS-based AC by chemical vapor deposition at 800°C for 70 min under the methane flow rate of 30 mL min^{-1} would be a candidate as an adsorbent for CO_2/CH_4 separation.

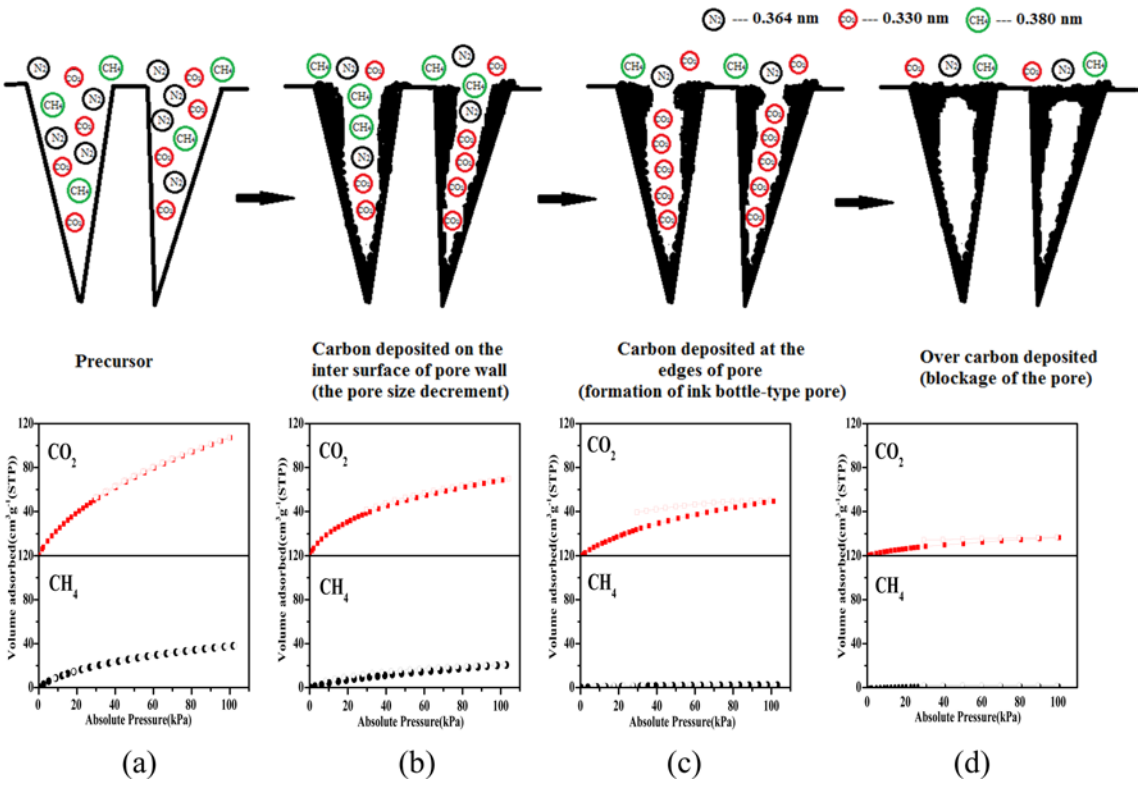

Fig. 13. Schematic model of CVD process on AC.

3.4. Adsorption-desorption rates

As the performance for PSA cycles are designed for kinetic separation, CMSs should have high adsorption and desorption rates [11]. In order to evaluate the CH_4 and CO_2 adsorption-desorption rates of CMS80070-30, a commercial cocoanut shell AC was also investigated for the comparison. The results are given in Figs. 11 and 12. It is found that CH_4 and CO_2 adsorption-desorption rates of CMS80070-30 is higher than that of commercial AC.

3.5. Schematic model for carbon deposition

Based on the above analysis, a schematic model for the process of carbon deposition on the SS-based ACs is shown in Fig. 13. Pretreated AC possesses pores with an average diameter of 1.21 nm, which can adsorb CH_4 and CO_2 molecules by pore filling (Fig. 13a). In Fig. 13b, carbons depositing on the inner surface of pore wall by methane decomposition decreases the average pore diameter to 0.54 nm, resulting in the decrease of both CH_4 and CO_2 adsorption capacity. However, the decrement of CO_2 adsorption capacity is lower compared to CH_4 due to the smaller molecular size of CO_2. When the pore size becomes too small to allow methane molecules entering, the carbon deposition on inner surface pore wall will stop (Fig. 13c). But the deposition can still perform at the edges of pore and leads to the formation of ink-bottle like pores, which allows CO_2 molecules entering. Finally, the deposited carbons block all pores in the matrix, and the adsorption capacity of CH_4 and CO_2 becomes very low (Fig. 13d).

4. Conclusions

CMSs were prepared by employing SS-based AC as a precursor via CVD using methane as a carbon source. Due to ZnS0.5 possesses more uniform microporous structure, it was chosen as a precursor to prepare CMSs under various conditions. The obtained CMSs were applied in the separation of CO_2/CH_4. It is demonstrated that increasing the deposition temperature, time and methane flow rate causes the decrease in the adsorption capacity of N_2, micropore volume and average pore diameter of CMSs. The CMSs obtained via CVD at 800°C for 70 min with the methane flow rate of 30 mL·min^{-1} gives the highest adsorption selectivity coefficient of 20.8 for CO_2/CH_4, which is expected to be a good candidate as an adsorbent for CO_2/CH_4 separation.

Conflict of Interest

No potential conflict of interest relevant to this article was reported.

Acknowledgements

This work is supported by the project for industrial key technology, Fujian Development & Reform Commission (2011-352), the National Science Foundation of China (21407025) and the National Science Foundation of Fujian Province he National Science Foundation of Fujian Province (2016J01047)".

References

[1] Deng Y, Xu J, Liu Y, Mancl K. Biogas as a sustainable energy source in China: regional development strategy application and decision making. Renewable Sustainable Energy Rev, **35**, 294 (2014). https://doi.org/10.1016/j.rser.2014.04.031.

[2] Weiland P. Biogas production: current state and perspectives. Appl Microbiol Biotechnol, **85**, 849 (2010). https://doi.org/10.1007/s00253-009-2246-7.

[3] Zhang Y, Sunarso J, Liu S, Wang R. Current status and development of membranes for CO_2/CH_4 separation: a review. Int J Greenhouse Gas Control, **12**, 84 (2013). https://doi.org/10.1016/j.ijggc.2012.10.009.

[4] Cavenati S, Grande CA, Rodrigues AE. Removal of carbon dioxide from natural gas by vacuum pressure swing adsorption. Energy Fuels, **20**, 2648 (2006). https://doi.org/10.1021/ef060119e.

[5] Bekkering J, Broekhuis AA, Van Gemert WJT. Optimisation of a green gas supply chain: a review. Bioresour Technol, **101**, 450 (2010). https://doi.org/10.1016/j.biortech.2009.08.106.

[6] Xing R, Ho WSW. Synthesis and characterization of crosslinked polyvinylalcohol/polyethyleneglycol blend membranes for CO_2/CH_4 separation. J Taiwan Inst Chem Eng, **40**, 654 (2009). https://doi.org/10.1016/j.jtice.2009.05.004.

[7] Liu D, Yi H, Tang X, Zhao S, Wang Z, Gao F, Li Q, Zhao B. Adsorption separation of CO_2/CH_4 gas mixture on carbon molecular sieves modified by potassium carbonate. J Chem Eng Data, **61**, 2197 (2016). https://doi.org/10.1021/acs.jced.5b00742.

[8] Wu Y, Yang Y, Kong XM, Li P, Yu JG, Ribeiro AM, Rodrigues AE. Adsorption of pure and binary CO_2, CH_4, and N_2 gas components on activated carbon beads. J Chem Eng Data, **60**, 2684 (2015). https://doi.org/10.1021/acs.jced.5b00321.

[9] Santos MPS, Grande CA, Rodrigues AE. Pressure swing adsorption for biogas upgrading. Effect of recycling streams in pressure swing adsorption design. Ind Eng Chem Res, **50**, 974 (2011). https://doi.org/10.1021/ie100757u.

[10] Yu HR, Cho S, Bai BC, Yi KB, Lee YS. Effects of fluorination on carbon molecular sieves for CH_4/CO_2 gas separation behavior. Int J Greenhouse Gas Control, **10**, 278 (2012). https://doi.org/10.1016/j.ijggc.2012.06.013.

[11] Foley HC. Carbogenic molecular sieves: synthesis, properties and applications. Microporous Mater, **4**, 407 (1995). https://doi.org/10.1016/0927-6513(95)00014-z.

[12] Miao Q, Tang Y, Xu J, Liu X, Xiao L, Chen Q. Activated carbon prepared from soybean straw for phenol adsorption. J Taiwan Inst Chem Eng, **44**, 458 (2013). https://doi.org/10.1016/j.jtice.2012.12.006.

[13] Kang HU, Kim WG, Kim SH. Pore size control through benzene vapor deposition on activated carbon. Chem Eng J, **144**, 167 (2008). https://doi.org/10.1016/j.cej.2008.01.017.

[14] Ahmad MA. Preparation of carbon molecular sieves from palm shell: effect of benzene deposition conditions. Adsorption, **15**, 489 (2009). https://doi.org/10.1007/s10450-009-9199-0.

[15] Cheng LH, Fu YJ, Liao KS, Chen JT, Hu CC, Hung WS, Lee KR, Lai JY. A high-permeance supported carbon molecular sieve membrane fabricated by plasma-enhanced chemical vapor deposition followed by carbonization for CO_2 capture. J Membr Sci, **460**, 1 (2014). https://doi.org/10.1016/j.memsci.2014.02.033.

[16] Atchudan R, Joo J, Pandurangan A. An efficient synthesis of graphenated carbon nanotubes over the tailored mesoporous molecular sieves by chemical vapor deposition. Mater Res Bull, **48**, 2205 (2013). https://doi.org/10.1016/j.materresbull.2013.02.048.

[17] Zhang T, Walawender WP, Fan LT. Preparation of carbon molecular sieves by carbon deposition from methane. Bioresour Technol, **96**, 1929 (2005). https://doi.org/10.1016/j.biortech.2005.01.026.

[18] Villar-Rodil S, Navarrete R, Denoyel R, Albiniak A, Paredes JI, Martínez-Alonso A, Tascón JMD. Carbon molecular sieve cloths prepared by chemical vapour deposition of methane for separation of gas mixtures. Microporous Mesoporous Mater, **77**, 109 (2005). https://doi.org/10.1016/j.micromeso.2004.08.017.

[19] Landers J, Gor GY, Neimark AV. Density functional theory methods for characterization of porous materials. Colloids Surf A Physicochem Eng Aspects, **437**, 3 (2013). https://doi.org/10.1016/j.colsurfa.2013.01.007.

[20] Pinto ML, Mestre AS, Carvalho AP, Pires J. Comparison of Methods to Obtain Micropore Size Distributions of Carbonaceous Materials from CO_2 Adsorption Based on the Dubinin−Radushkevich Isotherm. Ind Eng Chem Res, **49**, 4726 (2010). https://doi.org/10.1021/ie100080r.

[21] Chen Y, Li Z, Liu Q, Shen Y, Wu X, Xu D, Ma X, Wang L, Chen QH, Zhang Z, Xiang S. Microporous metal–organic framework with lantern-like dodecanuclear metal coordination cages as nodes for selective adsorption of C_2/C_1 mixtures and sensing of nitrobenzene. Cryst Growth Des, **15**, 3847 (2015). https://doi.org/10.1021/acs.cgd.5b00473.

[22] Qian Q, Machida M, Aikawa M, Tatsumoto H. Effect of $ZnCl_2$ impregnation ratio on pore structure of activated carbons prepared from cattle manure compost: application of N_2 adsorption-desorption isotherms. J Mater Cycles Waste Manage, **10**, 53 (2008). https://doi.org/10.1007/s10163-007-0185-x.

[23] Huang X, Cao JP, Zhao XY, Wang JX, Fan X, Zhao YP, Wei XY. Pyrolysis kinetics of soybean straw using thermogravimetric analysis. Fuel, **169**, 93 (2016). https://doi.org/10.1016/j.fuel.2015.12.011.

[24] Qian Q, Machida M, Tatsumoto H. Preparation of activated carbons from cattle-manure compost by zinc chloride activation. Bioresour Technol, **98**, 353 (2007). https://doi.org/10.1016/j.biortech.2005.12.023.

[25] Pezoti O, Cazetta AL, Bedin KC, Souza LS, Martins AC, Silva TL, Santos Júnior OO, Visentainer JV, Almeida VC. NaOH-activated carbon of high surface area produced from guava seeds as a high-efficiency adsorbent for amoxicillin removal: Kinetic, isotherm and thermodynamic studies. Chem Eng J, **288**, 778 (2016). https://doi.org/10.1016/j.cej.2015.12.042.

[26] Xing W, Liu C, Zhou Z, Zhang L, Zhou J, Zhuo S, Yan Z, Gao H, Wang G, Qiao SZ. Superior CO_2 uptake of N-doped activated carbon through hydrogen-bonding interaction. Energy Environ Sci, **5**, 7323 (2012). https://doi.org/10.1039/c2ee21653a.

[27] Veerakumar P, Chen SM, Madhu R, Veeramani V, Hung CT, Liu SB. Nickel nanoparticle-decorated porous carbons for highly active catalytic reduction of organic dyes and sensitive detection of Hg(II) ions. ACS Appl Mater Interfaces, **7**, 24810 (2015). https://doi.org/10.1021/acsami.5b07900.